



CHORUS

This is the accepted manuscript made available via CHORUS. The article has been published as:

Purcell effect in hyperbolic metamaterial resonators

Alexey P. Slobozhanyuk, Pavel Ginzburg, David A. Powell, Ivan Iorsh, Alexander S. Shalin, Paulina Segovia, Alexey V. Krasavin, Gregory A. Wurtz, Viktor A. Podolskiy, Pavel A. Belov, and Anatoly V. Zayats

Phys. Rev. B **92**, 195127 — Published 16 November 2015

DOI: [10.1103/PhysRevB.92.195127](https://doi.org/10.1103/PhysRevB.92.195127)

Purcell effect in Hyperbolic Metamaterial Resonators

Alexey P. Slobozhanyuk^{1,3*}, Pavel Ginzburg^{2,7**}, David A. Powell¹, Ivan Iorsh³, Alexander S. Shalin^{3,4,5}, Paulina Segovia², Alexey V. Krasavin², Gregory A. Wurtz², Viktor A. Podolskiy⁶, Pavel A. Belov³ and Anatoly V. Zayats²

¹Nonlinear Physics Center, Research School of Physics and Engineering, Australian National University, Canberra ACT 0200, Australia

²Department of Physics, King's College London, Strand, London WC2R 2LS, United Kingdom

³ITMO University, St. Petersburg 197101, Russia

⁴Kotel'nikov Institute of Radio Engineering and Electronics of RAS (Ulyanovsk branch), Ulyanovsk 432011, Russia

⁵Ulyanovsk State University, Ulyanovsk 432017, Russia

⁶Department of Physics and Applied Physics, University of Massachusetts Lowell, One University Ave, Lowell, MA, 01854, USA

⁷Department of Physical Electronics, Fleischman Faculty of Engineering, Tel Aviv University, Tel Aviv 69978, Israel

The radiation dynamics of optical emitters can be manipulated by properly designed material structures providing high local density of photonic states, a phenomenon often referred to as the Purcell effect. Plasmonic nanorod metamaterials with hyperbolic dispersion of electromagnetic modes are believed to deliver a significant Purcell enhancement with both a broadband and a non-resonant nature. Here, we have investigated finite-size resonators formed by nanorod metamaterials and shown that the main mechanism of the Purcell effect in such resonators originates from the supported hyperbolic modes, which stem from the interacting cylindrical surface plasmon modes of the finite number of nanorods forming the resonator. The Purcell factors delivered by these resonator modes reach several hundreds, which is up to 5 times larger than those in the epsilon-near-zero regime. It is shown that while the Purcell factor delivered by the Fabry–Pérot modes depends on the resonator size, the decay rate in the epsilon near-zero regime is almost insensitive to geometry. The presented analysis shows a possibility to engineer emission properties in structured metamaterials, taking into account their internal composition.

Corresponding authors: [*a.slobozhanyuk@phoi.ifmo.ru](mailto:a.slobozhanyuk@phoi.ifmo.ru), [**pginzburg@post.tau.ac.il](mailto:pginzburg@post.tau.ac.il)

1. Introduction

The local density of optical states (LDOS) related to various photonic modes can strongly affect quantum dynamics of light-matter interactions [1]. Free-space electromagnetic modes can be modified in the vicinity of material structures and, as a result, either a local enhancement or reduction of the interaction strength can be achieved. The rate of spontaneous emission in a weak light-matter coupling regime, calculated on the basis of the Fermi golden rule, is proportional to the LDOS and its change relative to free space is referred to as a Purcell factor [2]. Furthermore, the formalism of the Purcell effect can be generalized to higher-order effects, such as spontaneous two-photon emission [3,4]. The Purcell enhancement in dielectric cavities is typically related to the ratio of the quality factor of the resonance to the volume occupied by the resonant mode. Various types of photonic cavities can deliver quality (Q) factors as high as 10^{10} and satisfy the conditions to reach the strong coupling regime [5] where the Purcell factor description of decay dynamics breaks down [6]. Noble metal (plasmonic) nanostructures provide relatively low quality factors but yield sub-wavelength optical confinement [7] and, as a result, also efficiently influence spontaneous emission [8,9]. This nanoplasmonic approach is extremely beneficial for certain quantum optical applications, where improved and designed scattering cross-sections are required to develop functionalities at the nanoscale and single-photon levels [10]. The Purcell enhancement in plasmonic nanostructures depends significantly on the relative position of the emitters with respect to a metal nanostructure, posing serious challenges and limitations for large scale practical implementations [11]. Furthermore, the enhancement, based on local plasmonic resonances approach still have a limited bandwidth, even though it is much broader than for high-Q optical cavities.

A qualitatively different approach to decay rate engineering relies on designing the hyperbolic dispersion of modes supported by anisotropic metamaterials, which ensures high nonresonant Purcell factors in a broad wavelength range [12]. These metamaterials with extreme anisotropy of dielectric permittivity, also known as hyperbolic metamaterials, have recently

attracted significant attention due to their unusual electromagnetic properties. Homogenised hyperbolic metamaterials were theoretically shown to provide infinitely large LDOS and, as a result, are expected to deliver extremely high Purcell enhancements [13]. This diverging LDOS originates from the hyperbolic dispersion of modes in uniaxial crystals, having opposite sign of the permittivity components in the ordinary and extraordinary directions, perpendicular and parallel to the optical axis, respectively. The fundamental limitations for this type of enhancement result from a particular metamaterial realisation as composites of finite-length scale components, commonly referred to as “meta-atoms”[14], as well as the metamaterials’ nonlocal response [15,16]. The most widely used realizations of hyperbolic metamaterials are based on layered metal–dielectric structures [17] or vertically aligned nanorod arrays [18]. Hyperbolic metamaterials also served as building blocks for optical components with enhanced capabilities, such as hyperbolic cavities [19] and waveguides [20], as well as for delivering nonreciprocal effects [21], for Hamiltonian optics-based cavities [22], and many others.

In this work, we analyse emission properties of a radiating dipole embedded inside or in a close proximity of a finite-size three-dimensional resonator formed by a nanorod-based hyperbolic metamaterial. Taking into account the details of the hyperbolic metamaterial realization as a finite number of plasmonic nanorods, we show that the Purcell enhancement originates from Fabry–Pérot modes of the resonator formed by a hyperbolic metamaterial. The role of the modes of the metamaterial resonators on the Purcell factor was investigated for different resonator sizes, and the importance of the emitter’s position within the resonator has been considered. We also demonstrate the fast convergence of the Purcell enhancement with the increase of the number of nanorods in the array, with a 16x16 nanorod array having a properties of the infinite metamaterial slab (infinite number of finite length rods). This enables comparison of the Purcell enhancement provided by both finite-sized and infinite structures and separating the impact of the modal structure of finite-size resonators.

2. Effective medium theory and numerical modeling

We consider a metamaterial consisting of a square array of plasmonic (Au) nanorods (Fig. 1). This basic configuration enables addressing all the relevant effects, with substrate material and embedding dielectric material straightforwardly included in numerical modeling. In the first approximation, neglecting nonlocal effects [23], the optical response of such a structure can be obtained from a homogenization procedure of the nanorod composite [24], representing it as an effective uniaxial medium with permittivity tensor $\boldsymbol{\varepsilon} = \text{diag}(\boldsymbol{\varepsilon}_{xx}, \boldsymbol{\varepsilon}_{xx}, \boldsymbol{\varepsilon}_{zz})$, where $\boldsymbol{\varepsilon}_{xx} = \boldsymbol{\varepsilon}_{yy}$ and $\boldsymbol{\varepsilon}_{zz}$ are the permittivities for the light polarization perpendicular to and along the nanorod axes, respectively (Fig. 1(a, b)). In the frequency range where $\boldsymbol{\varepsilon}_{xx}$ and $\boldsymbol{\varepsilon}_{zz}$ have opposite signs (Fig. 1(c)), extraordinary electromagnetic modes, propagating in such an anisotropic medium, have hyperbolic dispersion. For the considered system, this crossing from conventional elliptic to hyperbolic dispersion regime occurs at around 520 nm wavelength where the real part of the effective permittivity $\boldsymbol{\varepsilon}_{zz}$ becomes vanishingly small (Fig. 1(c)). The frequency range around $Re(\boldsymbol{\varepsilon}_{zz}) = 0$ is called the epsilon near-zero (ENZ) regime. This ability to support a quasi-static behavior of electromagnetic waves (freeze phase) has various intriguing consequences on waves propagation in bended structures [25] and in tailoring radiation properties [26]. It should be noted, that ENZ regime is usually connected with the strong spatial dispersion effects, since vanishing leading term in the permittivity coefficient makes the next term of significant importance [27].

The nonlocal (spatial dispersion) behavior of the nanorod metamaterials cannot be described in the conventional effective medium theory and has impact on both reflection and transmission of the metamaterial as well as emission and nonlinear effects [23]. Electromagnetic nonlocalities could be classified as structural, material and collective [28]. While constitutive material components of the considered metamaterial may, in principle exhibit collective hydrodynamic-type nonlocalities [29], their contribution is small for the geometrical sizes considered here. Structural nonlocality due to the retardation effects in the unit cell is much stronger in the case

of nanorods metamaterial, requiring modifications in the homogenization approach and the use of modified effective medium models [30]. Numerical modelling which considers internal, microscopic structure of metamaterial composites, takes the structural nonlocality in the consideration automatically without the need of any additional considerations.

The numerical simulations have been performed using the time domain solver of the CST Microwave Studio 2014 package [31]. We used perfect matched layers (PML) boundary and additional space was added between the structure and the PMLs in order to prevent evanescent waves from interacting with the boundaries. Optical constants for gold were taken from Ref. [32]. The subwavelength dipolar emitter was modeled here as a perfect electric conductor (PEC) nanorod of length 28 nm and radius 1 nm (Fig. 1(b)). The Purcell factor was calculated through an input impedance of a point dipole source. As was previously shown [33, 34], this method is completely equivalent to the Green's function approach, which is widely used in photonics [35]. The overall number of mesh cells was around 3×10^6 with mesh density locally adjusted in order to accurately represent the source. In order to reach reliable results and to prevent the oscillation of the output time signal after the excitation has been turned off, the duration of the simulation is usually increased above the interval needed to transmit the excitation pulse.

The numerical analysis based on the Green function approach enables evaluation of both the decay rates which are proportional to the imaginary part of the Green function and the energy shift which is proportional to its real part [36]. Similar approach taking into account nonlocal response, Lamb shift and linewidth modifications were recently used for layered hyperbolic metamaterials [37]. The analysis, reported here, concentrates on Purcell factor evaluation. Since the rate enhancement has not shown extremely high values, wavelength shift was neglected for emitters.

3. Results

3.1. Hyperbolic metamaterial resonators.

We begin with analytical description of the modal structure of finite-size resonators made of homogenized hyperbolic metamaterial based on the nanorod assembly. The Purcell factor is proportional to the imaginary part of the Green's function in a medium [1]:

$$R(\omega) = \text{Im}G(\mathbf{r}, \mathbf{r}, \omega) \approx \text{Im} \sum_{n,l,m,\sigma} \frac{|E_x^{n,l,m,\sigma}(\mathbf{r})|^2}{\omega^2 - \omega_{n,l,m,\sigma}^2}, \quad (1.1)$$

where (n,l,m) are integers denoting the eigenmode number of the resonator made of the metamaterial, and $\sigma = \{\text{TE}, \text{TM}\}$ is the mode's polarization, where TE corresponds to the modes with the electric field lying in the xy plane and TM corresponds to the modes with the magnetic field in the xy plane. The imaginary part of electromagnetic Green's functions describes the LDOS and does not diverge due to losses in the system if the emitter is placed in lossless dielectric between the nanorods. On the other hand, material losses in the nanorods themselves and radiation from the resonator into the far-field remove divergence of Eq. 1.1 in the vicinity of the poles.

The rigorous eigenmode analysis of the anisotropic and lossy rectangular resonator requires sophisticated numerical techniques. However, approximate expressions for the eigen frequencies and field distributions in the resonator can be derived within an approximate analytical formalism [38]. Within this formalism, perfect electric conductor (PEC) boundary conditions are imposed at the side walls of the resonator at $x = \pm L_x / 2, y = \pm L_y / 2$ in order to obtain the resonator mode numbers, corresponding to quantized $k_{x,(m)}$ and $k_{y,(l)}$ wavevectors in x and y directions, respectively:

$$\begin{aligned} k_{x,(m)} &= \frac{\pi m}{L_x}, \quad m = 1, 3, 5 \dots \\ k_{y,(l)} &= \frac{\pi l}{L_y}, \quad l = 1, 3, 5 \dots \end{aligned} \quad (1.2)$$

If the radiating dipole is situated on the $(0,0,z)$ axis, only the modes with symmetric E_x and E_y field distributions with respect to inversions $x \rightarrow -x, y \rightarrow -y$ can be excited by the dipole and will contribute to the Purcell effect.

In order to obtain mode structure in the remaining z -direction, a slab waveguide is then considered which may support TM and TE guided modes confined in z -direction. The propagation constant of these modes $k_{\perp,(m,l)}$ satisfies the condition

$$k_{\perp,(m,l)} = \sqrt{k_{x,(m)}^2 + k_{y,(l)}^2}. \quad (1.3)$$

This $k_{\perp,(m,l)}$ propagation constant can be evaluated by finding the modes of a hyperbolic-metamaterial-slab waveguide in the effective medium approximation [39]. As has been shown in the analysis of the metamaterial waveguides [39], and can also be seen from the numerical modeling below, this approximation holds for lower-order highly confined modes of sufficiently large resonators.

First, we will consider quasi-TE modes of the resonator. By substituting Eq. (1.2) into the dispersion equation Eq. (1.3) for a slab waveguide which is symmetric with the respect to the $z \rightarrow -z$ inversion, we find two classes of modes with the tangential electric field either symmetric ($n=0,2,4,\dots$) or antisymmetric ($n=1,3,5,\dots$) along the z axis, respectively (the index here corresponds to the number of zero crossings for a leading field component: electric field for TE and magnetic field for TM modes):

$$\frac{\sqrt{k_{\perp,(m,l)}^2 - \left(\frac{\omega_{m,l,n,TE}}{c}\right)^2}}{\sqrt{\epsilon_{xx} \left(\frac{\omega_{m,l,n,TE}}{c}\right)^2 - k_{\perp,(m,l)}^2}} = \tan \left(\frac{\sqrt{\epsilon_{xx} \left(\frac{\omega_{m,l,n,TE}}{c}\right)^2 - k_{\perp,(m,l)}^2} L_z}{2} + \frac{\pi}{4} (1 - (-1)^n) \right). \quad (1.4)$$

If the dipole is placed at $z = 0$, the antisymmetric modes will have the node of the electric field at the dipole position and thus cannot be excited and will not contribute to the Purcell effect (Eq. 1). When the dipole is shifted from the $z = 0$, both symmetric and antisymmetric modes will contribute to the Purcell factor. Similarly, using the waveguide dispersion for TM polarized modes, we obtaine

$$\frac{\sqrt{\epsilon_{xx}} \sqrt{k_{x,(m)}^2 + k_{y,(l)}^2 - \left(\frac{\omega_{m,l,n,TM}}{c}\right)^2}}{\sqrt{\left(\frac{\omega_{m,l,n,TM}}{c}\right)^2 - \frac{k_{\perp,(m,l)}^2}{\epsilon_{zz}}}} = \tan \left(\frac{\sqrt{\epsilon_{xx}} \sqrt{\left(\frac{\omega_{m,l,n,TM}}{c}\right)^2 - \frac{k_{\perp,(m,l)}^2}{\epsilon_{zz}}}}{2} L_z + \frac{\pi}{4} (1 - (-1)^n) \right), \quad (1.5)$$

In this case, however, the modes are symmetric ($n = 0, 2, 4, \dots$) or antisymmetric ($n = 1, 3, 5, \dots$) with respect to the tangential component of the magnetic field, with the electric field having opposite symmetry.

In order to distinguish the mode contributions to the Purcell effect, the spectrum of the eigenmodes will be first analyzed assuming vanishing Ohmic losses in the metamaterial. In this approximation, following Eq. (1.4), the TE mode eigenfrequencies are limited by

$$\frac{\pi}{L_x} \sqrt{(m)^2 + (l)^2} < \frac{\omega_{m,l,n,TE}}{c} < \frac{\pi}{L_x} \sqrt{\epsilon_{xx}} \sqrt{(m)^2 + (l)^2}, \quad (1.6)$$

satisfying the requirement that the left hand side of Eqs. (1.2, 1.4) should be real-valued. Therefore, for any finite frequency range, only a finite number of pairs (m, l) exists that satisfy Eq.(1.6). For each (m, l) pair, a finite set of mode numbers n can be found from the solution of Eq.(1.3). Thus, in a finite frequency range, only a finite number of eigenmodes (m, l, n) of the metamaterial resonator exists.

Specifically, for the metamaterial resonator of the square cross-section with $L_x=L_y = 900$ nm and $L_z= 350$ nm and the effective permittivity as in Fig. 1 (c), the following eigenmodes can be excited in the spectral range from 500 to 1500 nm: TE_{110} at $\lambda=1450$ nm, TE_{130} and TE_{310} at $\lambda= 780$ nm, and TE_{330} at $\lambda= 570$ nm. It should be noted that while the predicted higher-order modes were

observed in the rigorous numerical simulations of the nanorod composite, the fundamental mode in the vicinity of 1450 nm has not been observed and occurs at wavelengths larger than 1500 nm (Fig. 2). This is a known discrepancy [40] related to the fact that the simplified analysis used above works worse for the fundamental modes with lower confinement within a resonator, and thus the actual frequency of the TE₁₁₁ mode frequency can deviate substantially from the value predicted by the simplified analytical formalism.

Contrary to TE modes, the eigenfrequencies of TM modes decrease with the increase of m and l as can be seen from Eq. (1.5). This property of the hyperbolic resonators has been observed both theoretically and experimentally [19], and can be understood from the requirement for the TM eigenfrequencies analogous to Eq. (1.6):

$$\frac{\pi^2}{L_x^2}[m^2 + l^2] > \frac{\omega_{m,l,n,\text{TM}}^2}{c^2} > \frac{\pi^2}{L_x^2 \epsilon_{zz}} [(m)^2 + l^2]. \quad (1.7)$$

Since ϵ_{zz} is negative in the hyperbolic regime, the right-hand-side inequality holds for any frequency and m, l . Thus, there exist modes with arbitrary large m, l that satisfy the left-hand-side inequality. The number of the supported modes is however limited due to the metamaterial realization as a periodic nanorod array. Contrary to the case of the uniform hyperbolic metamaterial, the x and y wavevectors should be within the first Brillouin zone of the array, $k_{x,y} < \pi/a$, where a is the period of the array. Thus, for TM modes, m and l eigenvalues can be 1, 3, 5, and 7 in the case of the 16x16 nanorod array with the parameters as in Fig. 1. For simplicity, in these analytical calculations we do not consider possible coupling between TE and TM modes due to three-dimensional geometrical confinement (the numerical modelling include all the effects).

For each value of m and l there is a number of eigenmodes corresponding to different n . This number is finite and increases with m, l . Despite a large number of the TM polarized eigenmodes supported by the resonator, many of them have a minor contribution to the overall Purcell factor,

since those modes are either characterized by small Q-factors, due to the large damping inside the resonator when the losses in metal are considered, or by a small value of x-component of the electric field at the dipole's position, due to the different symmetry properties of the eigenmodes. Namely, some of the eigenmodes would have minimum of the x component of the electric field at the dipole position and some would have maxima [41]. Moreover, in the vicinity of the ENZ frequency, the modes with large values of n are excited. However, these modes have large losses and, thus, give little contribution to the overall Purcell effect. It should be noted, however, that calculations of the Purcell enhancement for emitters placed in the contact with lossy media, face several challenges as the Green's functions diverge [30]. This problem is usually addressed by introducing a depolarization volume (a small lossless cavity) around the emitter [30]. The numerical modeling below does not, however, face the above issues, as the emitter is placed in the lossless space between actual rods, forming the metamaterial.

The dependences of the resonant wavelength on the resonator height L_z for three modes TE_{130} , TM_{151} , and TM_{551} are shown in Figure (3a). The higher-order mode TM_{551} is lower in frequency than the lower order mode TM_{151} as is expected for the hyperbolic resonators. This can be intuitively understood considering PEC boundary conditions on the interface perpendicular to the z axis. In this case, k_z is simplified to $k_z = \pi n L_z = \sqrt{\epsilon_{xx}} \sqrt{\omega^2 / c^2 - k_{\perp}^2 / \epsilon_{zz}}$, where n is an integer. It can be seen that for fixed n , the eigenfrequency decreases with increasing k_{\perp} . The dependence of the resonant wavelength on the resonator width L_x at the fixed resonator length $L_z = 350$ nm is shown in Figure (3b). As we can see, the resonant wavelengths of the TM modes decrease with the increase of the resonator lateral size. This behavior is evident from Eq. (1.3), since it can be seen that for the fixed value of k_z^{TM} the resonant frequency should increase with increasing L_x . In contrast, the wavelengths of the TE modes increase with the increase of the resonator width L_x similar to the case of a conventional anisotropic dielectric resonator.

3.2. Purcell enhancement due to the hyperbolic resonator modes

The analytical analysis performed above does not account for either the microscopic structure of the metamaterial or the radiation from the resonator. We now compare the effective medium analytical description to the results of the numerical modeling in the case of an x-polarized dipole placed in the centre of the 16x16 array of Au nanorods (period $a = 60$ nm and radius $r = 15$ nm) which corresponds to the resonator dimensions $L_y = L_x = 900$ nm and $L_z = 350$ nm. We have considered real losses in gold for comparison to the analytical model as well as artificial low losses (artificially reduced in 10 times) in order to articulate the mode position (Fig. 2). The analytical model provides a clear correspondence to the numerical results and the individual eigenmodes can be identified. The highest Purcell factor corresponds to the excitation of the TM_{551} eigenmode in the vicinity of 1000 nm. The Purcell factor near the ENZ frequency range does not have extremely large values, as would be expected in the case of an infinitely large metamaterial [30].

3.3. Saturation of the Purcell enhancement in finite size arrays

The Purcell factor for the electric dipole placed in the centre of the metamaterial resonator was numerically calculated for different sizes of the resonator (Fig. 4). Both parallel and perpendicular to the nanorods orientations of the emitting dipole were analysed in square and rectangular resonators with up to 18 rods in one direction. The obtained dependence of the Purcell factor shows a fast convergence with an increasing number of rods in the array. In fact, in the arrays larger than 16x16 rods (900x900 nm), the Purcell factor approaches the values for the infinite (in x and y directions) planar metamaterial slab, so that the Purcell factor for 16x16 and 18x18 arrays is essentially the same without the signatures of the resonant modes of the resonator due to the reduced quality factor of the modes (Fig. 4(a)). This quality factor reduction in larger systems is the result of increased material losses due to the mode spread over larger number of rods. Rectangular nanorod

arrays show similarly fast convergence, enabling to state that the behavior of 16x16 nanorod structures is extremely close to that of the infinite metamaterial (Fig. 4(a)). In particular, the x -oriented dipole source which is located in the central part of the array can excite only even modes (Fig. 4(a)). It can be seen that for the 2x2 array the highest Purcell factor (around 500) is reached at 950 nm wavelength (due to the small number of the rods forming the resonator, the identification of the mode structure of the resonator is not possible in the effective medium formalism as in Section 3.1). The highest Purcell factor obtained for the smallest array can be attributed to a small modal volume. For larger arrays this mode exhibits a slight shift to longer wavelengths as expected from Eq. (1.4), and the Purcell factor decreases up to the value of 200. The Purcell factor for a z -oriented dipole is very low but also follows the mode structure of the resonator with the increase of number of rods (Fig. 4(b)). The rectangular nanorod arrays provide a Purcell factor of around 200 already for 2 rows of nanorods (Fig. 4(c)). The contribution of different transverse modes of the rectangular array in the Purcell factor is more pronounced for the arrays with smaller number of rows and becomes indistinguishable for the arrays with 6 or more rows of rods (Fig. 4 (c), green curve). For all considered sizes of the resonators, a Purcell factor of less than 100 is observed in the ENZ regime, at around 520 nm wavelength (Fig. 1(c)). As one can see from the consideration of rectangular metamaterial resonators, the optical response of the finite-size resonators converges fast to the response of the infinitely extended metamaterial slabs.

3.4. Purcell enhancement dependence on the rods length

We will now investigate the impact of the resonator height (rod length) on the Purcell factor (Fig. 5). In this section, the resonators made of an array of 16x16 rods were considered. For all nanorod heights, there is a relatively small peak in the vicinity of the ENZ frequency related to the high modal density of bulk plasmon-polariton modes at this frequency [39,42]. The highest observed Purcell factor strongly depends on the rod length. Its maximum shifts to longer wavelengths with the increase in rod height, in accordance with the frequency shift of the resonator mode (Eq. 1.4). This

(TM_{551}) mode has a characteristic field distribution inside the resonator (Fig. 5(b)) with three pronounced maxima of the electric field (2 maxima of the magnetic field with one zero-crossing), typical of the 2nd Fabry-Perot TM mode along the rods. Away from the modes of the resonator, the electric field has a characteristic cross-shaped form (Fig. 5 (c)) typical for a radiating dipole field distribution in a hyperbolic dispersion regime [12].

3.5. Purcell enhancement in small hyperbolic resonators.

If, starting from a single nanorod, the number of rods in the resonator is gradually increased, a nontrivial behaviour of the Purcell factor is observed (Fig. 6). The highest Purcell factor is obtained neither with a single rod nor in the limit of an infinite number of rods. The optimal structure provides a resonant mode with a high LDOS which enhances the decay rate. It can be seen that the dipole positioned near the centre of a single nanorod excites the second-order mode $n=2$ with three maxima of the electric field (Fig. 6(b)) at the wavelength of around 855 nm and the fourth mode $n=4$ with five field maxima (Fig. 6(c)) at the wavelength of around 610 nm. Adding more nanorods to the resonator, and, thus, changing its size and the modal structure, leads to the shift of the resonant frequencies in the red spectral range, in accordance with Eq. 1.4. In particular, for the geometry with four nanorods, the second mode is excited at a wavelength of ca. 940 nm (Fig. 6(d)) and the fourth at a wavelength of ca. 640 nm (Fig. 6(e)). As mentioned above, the dipole located near the middle section of the nanorod layer can only couple to even modes.

3.6. Purcell enhancement dependence on the dipole position.

In order to understand the average Purcell factor for an ensemble of randomly distributed emitters, the position-dependent Purcell factor has been investigated. When the position of the emitter is changed along the nanorod length from just outside the metamaterial towards the centre of the metamaterial layer, the Purcell factor has four maxima, which correspond to the four lowest modes of the resonator (Fig. 7). The odd modes were not excited by the dipole situated at the

central point of the array due to symmetry-induced selection rules. It can be seen from the LDOS spectrum (Fig. 7(a)) that the efficiency of the excitation of the resonator modes depends on the local field strength of a particular mode at the position of the radiating dipole. It can be seen that at different dipole position, preferential excitation of the modes TM_{130} (2 electric field maxima, one magnetic field maximum, no magnetic field zero-crossing), TM_{551} (3 electric field maxima, 2 magnetic field maxima, 1 magnetic field zero-crossing), and TM_{552} (4 electric field maxima, 3 magnetic field maxima, 2 magnetic field zero-crossing) occurs at the wavelengths of 1363 nm, 1000 nm and 750 nm, respectively. For the shorter wavelength of 600 nm, the electric field is shaped as an inverted “V” (Fig. 7(e)), typical to the nonresonant hyperbolic regime. The Purcell factor drops off very quickly with increasing the distance between the dipole and the metamaterial surface: dipoles situated more than 20 nm away from the interface do not exhibit any significant Purcell enhancement (Fig. 7).

4. Conclusion

A comprehensive numerical and analytical analysis of the Purcell enhancement in finite-size nanorod metamaterial resonators was performed. Using a nanorod metamaterial with hyperbolic dispersion of electromagnetic modes, the resonators with a complex hierarchy of modes can be realized. We have shown that the modes of the hyperbolic resonator are responsible for the enhancement of spontaneous emission rates of emitters placed inside the resonator. Thus, a controllable Purcell enhancement can be achieved in the desired wavelength range by choosing appropriate resonator sizes. Detailed analysis of various types of geometrical arrangements of the metamaterial and emitter were carried out. The results suggest that finite-size metamaterial resonators with properly designed modes outperform infinite metamaterials in terms of radiation efficiency enhancement. It was shown that the influence of only 16x16 nanorod array on the dipole emission properties converges to that of an infinite metamaterial. Our work can provide guidelines for modeling and

optimization of experimental samples. As for an outlook for possible future applications, it is worth mentioning nanostructured light-emitting devices with high-speed switching rates, cavities for surface plasmon amplification by stimulated emission of radiation (SPASERs), and sensing applications.

Acknowledgments:

This work has been supported, in part, by EPSRC (UK), the ERC iPLASMM project (321268), US Army Research Office (W911NF-12-1-0533) and Australian Research Council. APS acknowledges support via the SPIE Scholarship. A. P. S., D. A. P. acknowledge support Australian Research Council (Australia). P.S.O. is grateful for the support from CONACYT. G.W. acknowledges support from the EC FP7 project 304179 (Marie Curie Actions). A.Z. acknowledges support from the Royal Society and the Wolfson Foundation and rejects any involvement in the grants, listed below. The work of I. I., A. S. S, P. A. B. was supported by the Ministry of Education and Science of the Russian Federation, by the Government of the Russian Federation (Grant 074-U01), by Russian Fund for Basic Research (N13-02-00623) and the Dynasty Foundation (Russia). I. I. acknowledges Grant of the President of Russian Federation (MK-5220.2015.2). A. S. acknowledges Russian Foundation for Basic Research (Projects No. 14-02-31783).

Figure Captions

Figure 1. (Colour online) (a) Schematic view of the hyperbolic metamaterial resonator with the transverse dimensions L_x and L_y . (b) Schematics of the numerical setup. An emitting dipole is inserted in the centre of the resonator. (c) The effective permittivity of the metamaterial calculated for an infinite array of nanorods with $L_z = 350$ nm, $a = 60$ nm, $r = 15$ nm (Au permittivity was taken from [32]).

Figure 2. (Colour online) The comparison of the numerical (red and blue lines) and analytical (green and black lines) of the Purcell factor in the case of real losses (solid lines) and reduce losses $\text{Im}(\epsilon)/10$

(dashed lines). The metamaterial parameters are as in Fig. 1. The resonator size is 16x16 nanorods with $L_x = L_y = 900$ nm.

Figure 3. (Colour online) Dependence of the resonant wavelength of the eigenmodes on (a) L_z for the fixed $L_x = L_y = 900$ nm and (b) L_x for fixed $L_z = 350$ nm. Error bars indicate the width of the resonance.

Figure 4. (Colour online) The Purcell factor dependence on the number of nanorods in square (a,b) and rectangular (c) lattices for an emitting dipole perpendicular (a,c) and parallel (b) to the nanorods. The dipole is located in the centre of the array.

Figure 5. (Colour online) (a) The Purcell factor dependence on the height of the hyperbolic metamaterial resonator (16x16 nanorod array, $L_x = L_y = 900$ nm). (b,c) The electric field (E_x) distributions excited by the dipole positioned at the centre of the resonator with $L_z = 350$ nm, at the wavelength of (b) 1000 nm and (c) 600 nm (nonresonant wavelength).

Figure 6. (Colour online) (a) Comparison of the Purcell factor for different numbers of plasmonic rods forming a resonator. Electric fields (E_x) of the dipole near a single nanorod (b,c) and near four nanorod array (d,e) at the wavelengths of 856 nm (b), 611 nm (c), 937 nm (d) and 637 nm (e).

Figure 7. (Colour online) (a) The Purcell factor dependence on an emitter position inside the metamaterial resonator with $L_z = 350$ nm and $L_x = L_y = 900$ nm. The coordinate $z=0$ corresponds to the edge of the hyperbolic medium. (b-e) The electric field (E_x) distributions excited by the dipole positioned at the $z = 0$ for the wavelengths of (b) 1363 nm (TM₁₃₀ mode, 1st Fabry-Perot resonance $n=0$, with 2 electric field maxima, one magnetic field maximum, no magnetic field zero-crossing), (c) 1000 nm (TM₅₅₁ mode, 2nd Fabry-Perot resonance $n=1$ with 3 electric field maxima, 2 magnetic field maxima, 1 magnetic field zero-crossing), (d) 750 nm (TM₅₅₂ mode, 3rd Fabry-Perot resonance $n=2$

with 4 electric field maxima, 3 magnetic field maxima, 2 magnetic field zero-crossing), and (e) 600 nm (nonresonant wavelength). All other parameters as in Fig. 3.

List of Figures

Figure 1

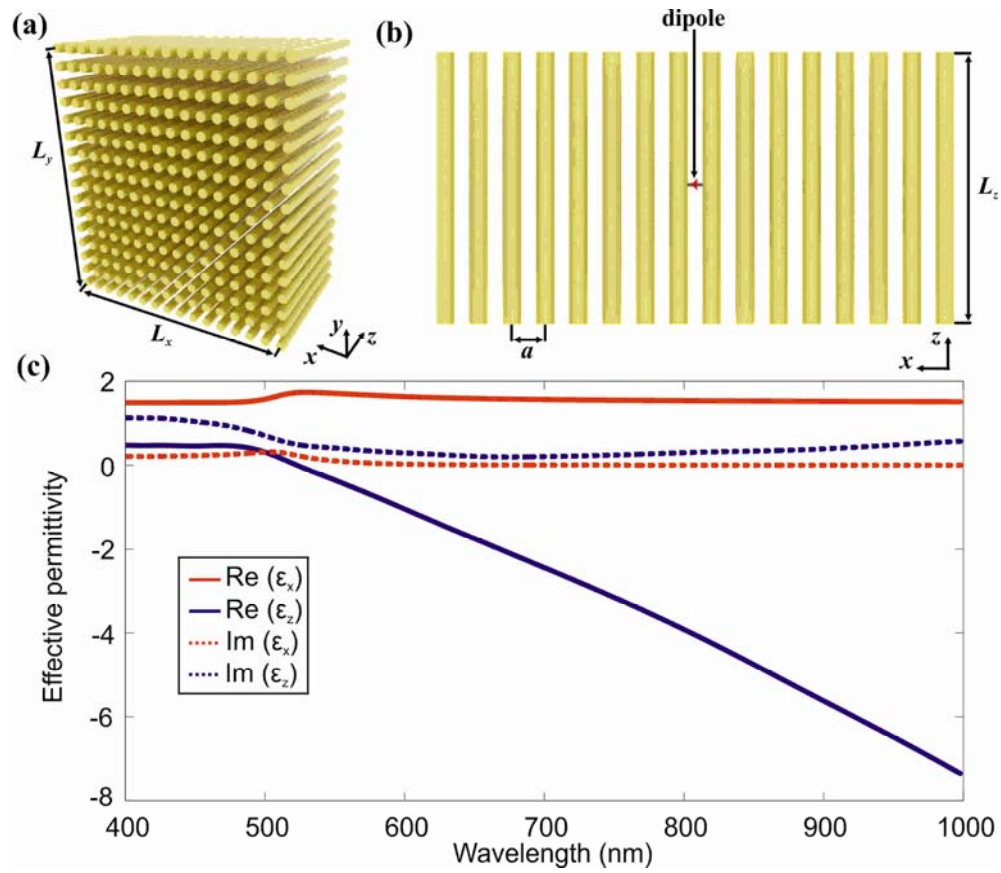


Figure 2

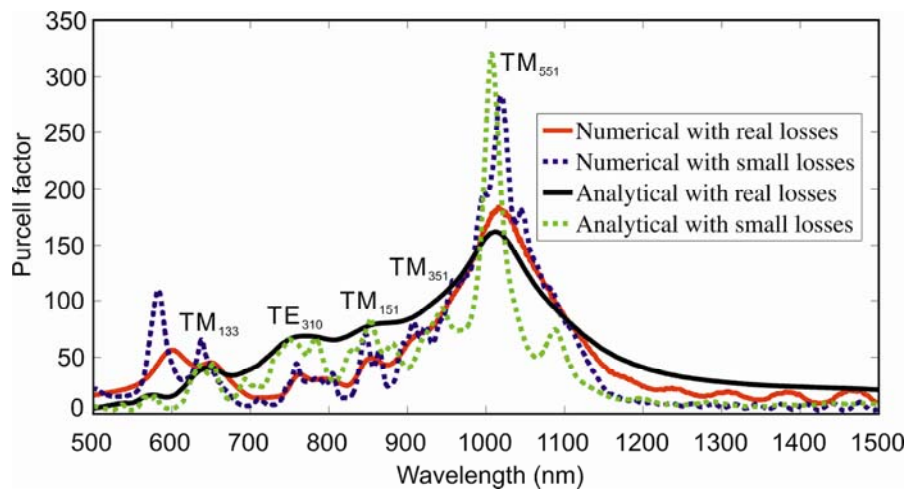


Figure 3

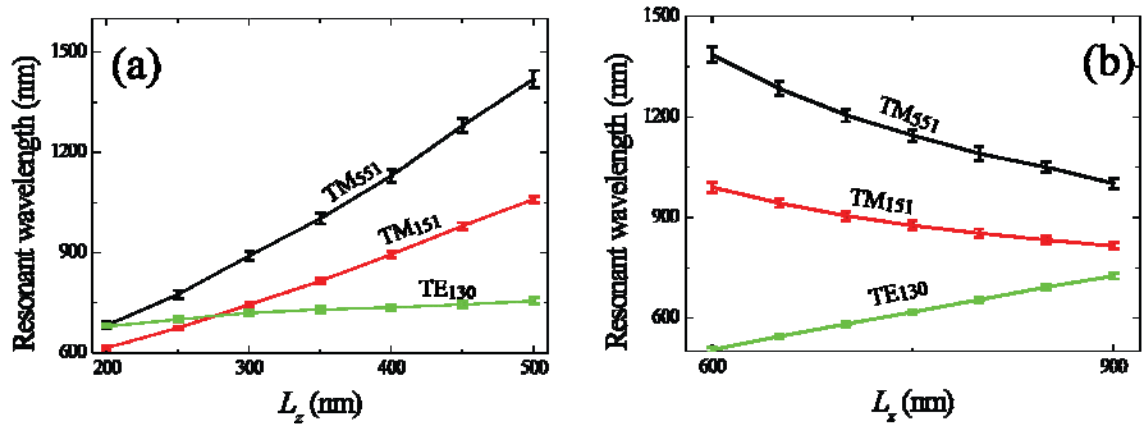


Figure 4

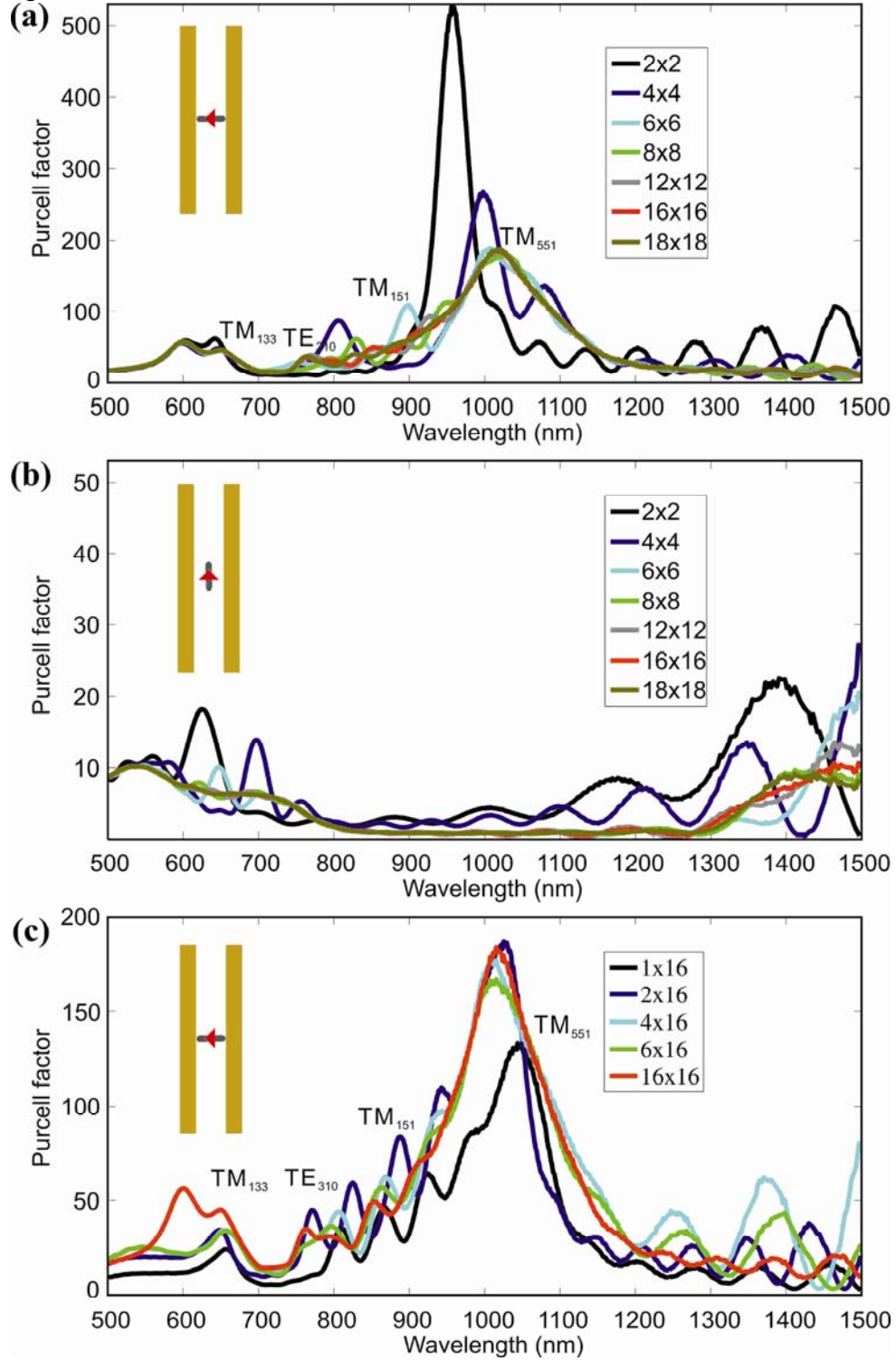


Figure 5

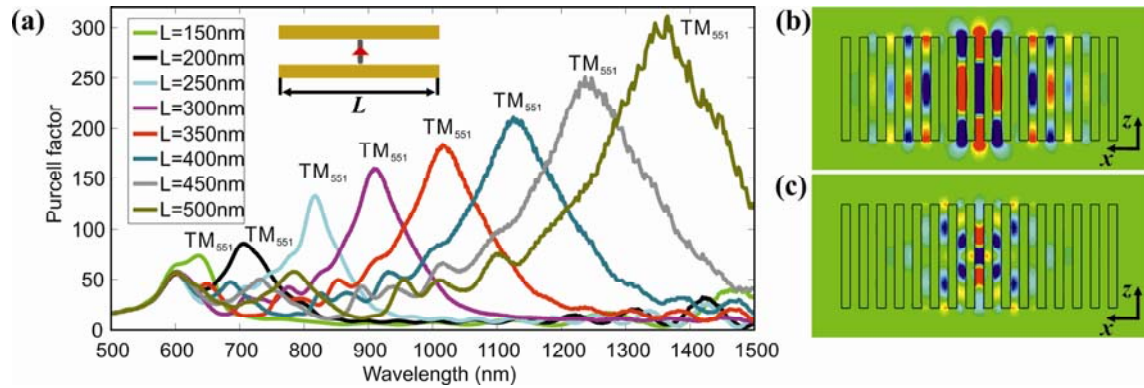


Figure 6

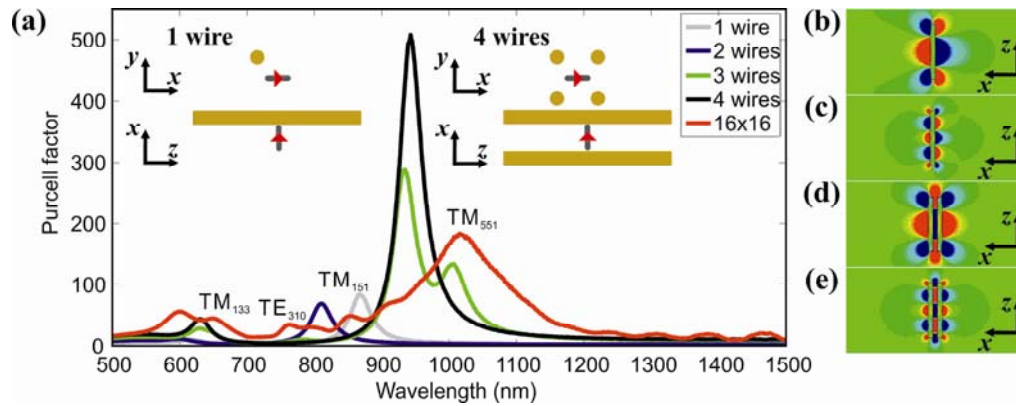
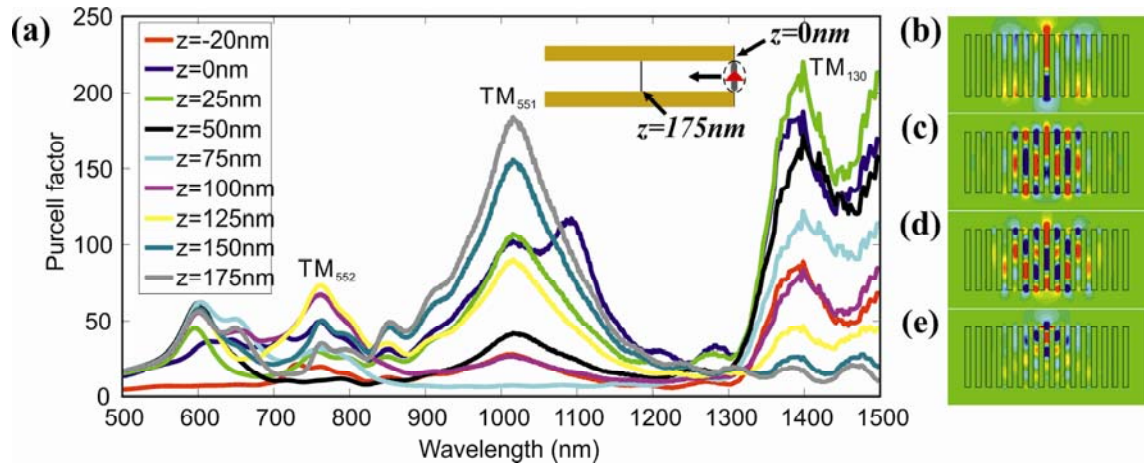


Figure 7.



References:

1. L. Novotny and B. Hecht, *Principles of Nano-Optics* (Cambridge University Press 2006).
2. E. M. Purcell, Phys. Rev. **69**, 681 (1946).
3. A. Hayat, P. Ginzburg, and M. Orenstein, Phys. Rev. Lett. **103**, 023601 (2009).
4. A. N. Poddubny, P. Ginzburg, P. A. Belov, A. V. Zayats, and Y. S. Kivshar, Phys. Rev. A **86**, 033826 (2012).
5. K. J. Vahala, Nature **424**, 839-846 (2003).
6. P. Ginzburg, A. V. Krasavin, D. Richards, and A. V. Zayats, Phys. Rev. A **90**, 043836 (2014).
7. D. K. Gramotnev and S. I. Bozhevolnyi, Nature Photon. **4**, 83 - 91 (2010).
8. L. Novotny and N. van Hulst, Nature Photon. **5**, 83–90 (2011).
9. J.-J. Greffet, Science **308**, 1561-1563 (2005).
10. A. V. Akimov, A. Mukherjee, C. L. Yu, D. E. Chang, A. S. Zibrov, P. R. Hemmer, H. Park, and M. D. Lukin, Nature **450**, 402-406 (2007).
11. A. G. Curto, G. Volpe, T. H. Taminiau, M. P. Kreuzer, R. Quidant, N. F. van Hulst, Science **329**, 930 (2010).
12. P. Shekhar, J. Atkinson, Z. Jacob, Nano Convergence **1**:14, 2014.
13. Z. Jacob, J. Kim, G. V. Naik, A. Boltasseva, E. E. Narimanov, and V. M. Shalaev, Appl. Phys. B **100**, 215 (2010).
14. A. N. Poddubny, P. A. Belov, P. Ginzburg, A. V. Zayats, and Y. S. Kivshar, Phys. Rev. B **86**, 035148 (2012).
15. W. Yan, M. Wubs, and N. A. Mortensen, Phys. Rev. B **86**, 205429 (2012).
16. T. Tümkür, G. Zhu, P. Black, Yu. A. Barnakov, C. E. Bonner, and M. A. Noginov, Appl. Phys. Lett. **99**, 151115 (2011).
17. H. N. S. Krishnamoorthy, Z. Jacob, E. Narimanov, I. Kretschmar, and V. M. Menon, Science **336**, 205–209 (2012).
18. P. Ginzburg, F. J. Rodríguez Fortuño, G. A. Wurtz, W. Dickson, A. Murphy, F. Morgan, R. J. Pollard, I. Iorsh, A. Atrashchenko, P. A. Belov, Y. S. Kivshar, A. Nevet, G. Ankonina, M. Orenstein, and A. V. Zayats, Opt. Express **21**, 14907-14917 (2013).
19. X. Yang, J. Yao, J. Rho, X. Yin, and X. Zhang, Nat. Photonics **6**, 450 (2012).
20. Y. He, S. He and X. Yang, Opt. Lett. **37**, 2907–2909 (2012).
21. A. Leviyev, B. Stein, T. Galfsky, H. Krishnamoorthy, I. L. Kuskovsky, V. Menon, A. B. Khanikaev, ArXiv e-prints (2015), arXiv: 1505.05438
22. Zhiyuan Sun, Á. Gutiérrez-Rubio, D. N. Basov, and M. M. Fogler, Nano Lett. **15** (7), 4455–4460 (2015).
23. B. M. Wells, A. V. Zayats, and V. A. Podolskiy, Phys. Rev. B **89**, 035111 (2014).
24. J. Elser, R. Wangberg, V. A. Podolskiy, and E. Narimanov, Appl. Phys. Lett. **89**, 261102 (2006)
25. M. Silveirinha, N. Engheta, Phys. Rev. Lett. **97**, 157403 (2006).
26. Alù, M. Silveirinha, A. Salandrino, N. Engheta, Phys. Rev. B **75**, 155410 (2007).
27. E. Forati and G. W. Hanson, New J. Phys. **15**, 123027 (2013).
28. P. Ginzburg and A. V. Zayats, ACS Nano **7**, 4334–4342 (2013).
29. N. A. Mortensen, S. Raza, M. Wubs, T. Sondergaard, and S. I. Bozhevolnyi, Nat. Commun. **5**, 3809 (2014).
30. V. Podolskiy, P. Ginzburg, B. Wells and A. Zayats, Faraday Discussions **178**, DOI: 10.1039/C4FD00186A (2014).
31. www.cst.com
32. P. B. Johnson, R. W. Christy, Phys. Rev. B **6**, 4370–4379, (1972).
33. A. P. Slobozhanyuk, A. N. Poddubny, A. E. Krasnok, and P. A. Belov, Appl. Phys. Lett. **104**, 161105 (2014).
34. A. E. Krasnok, A. P. Slobozhanyuk, C. R. Simovski, S. A. Tretyakov, A. N. Poddubny, A. E. Miroshnichenko, Y. S. Kivshar, and P. A. Belov, Sci. Rep. **5** (2015).
35. M. Agio and A. Alu, *Optical Antennas* (Cambridge University Press, 2013).
36. W. Vogel and D.-G. Welsch, Quantum Optics, 3rd, Revised and Extended Edition (Wiley-VCH, 2006).
37. F. Intravaia and K. Busch, Phys. Rev. A **91**, 053836 (2015).
38. A. K. Okaya and L. F. Barash, Proc. IRE **50**, 2081–2092 (1962).
39. N. Vasilantonakis, M. Nasir, W. Dickson, G. A. Wurtz, A. V. Zayats, Laser Phot. Rev. **9**, DOI: 10.1002/lpor.201400457 (2015).
40. R. K. Moniga and A. Ittipiboon, IEEE Transactions on Antennas and Propagation **45**, 1348-1356 (1997).
41. F. Lemoult, M. Fink, G. Lerosey, Nat. Commun. **3**, 889 (2012).

42 S.V. Zhukovsky, O. Kidwai, and J. E. Sipe, Optics Express **21**, 14982 (2013).